

TWISTING OF X-RAY ISOPHOTES IN TRIAXIAL GALAXIES

Aaron J. Romanowsky

Christopher S. Kochanek

Harvard-Smithsonian Center for Astrophysics, MS-10,

60 Garden Street, Cambridge MA 02138

Email: aromanowsky@cfa.harvard.edu

ABSTRACT

We investigate X-ray isophote twists created by triaxiality differences between the luminous stellar distributions and the dark halos in elliptical galaxies. For a typically oblate luminous galaxy embedded in a more prolate halo formed by dissipationless collapse, the triaxiality difference of $\Delta T \simeq 0.7$ leads to typical isophote twists of $\langle \Delta\psi_X \rangle \simeq 16^\circ \pm 19^\circ$ at 3 stellar effective radii. In a model which includes baryonic dissipation the effect is smaller, with $\Delta T \simeq 0.3$ and $\langle \Delta\psi_X \rangle \simeq 5^\circ \pm 8^\circ$. Thus, accurate measurements of X-ray isophote twists may be able to set constraints on the interactions between baryons and dissipationless dark matter during galaxy formation. The 30° X-ray isophote twist in the E4 galaxy NGC 720 cannot be reproduced by our model, suggesting an intrinsic misalignment between the halo and the stars rather than a projection effect.

Subject headings: galaxies: elliptical and lenticular, cD — galaxies: formation — galaxies: structure — galaxies: fundamental parameters — galaxies: individual (NGC 720) — X-rays: galaxies — dark matter

1. INTRODUCTION

Determining the intrinsic shapes of the luminosity and mass distributions of elliptical galaxies is an important unresolved problem. Both observational constraints from individual systems and predictions from theory demonstrate that the stellar and dark matter components of ellipticals are well described as triaxial ellipsoids. Parametric (e.g., Ryden 1992; Lambas, Maddox, & Loveday 1992) and non-parametric (Fasano & Vio 1991; Tremblay & Merritt 1995; Ryden 1996) inversions of the ellipticity distribution of the stellar components rule out the hypotheses that elliptical galaxies are all oblate or all prolate. Because of the information lost in projection, inversions that include triaxiality cannot determine a unique shape distribution, but the ellipticals seem to fall into two classes: bright ($M_B < -20$), triaxial, boxy galaxies and faint, roughly oblate, disk galaxies (Tremblay & Merritt 1996). This division is consistent with other structural, dynamical, and evolutionary evidence for two classes of ellipticals (e.g., Fasano 1991; Fasano & Vio 1991; Busarello, Longo, &

Feoli 1992; Capaccioli, Caon, & D’Onofrio 1992; Nieto, Poulain, & Davoust 1994; Jørgensen & Franx 1994; Kormendy & Bender 1996).

Binney (1978, 1985; see also Contopoulos 1956) first noted that a triaxial galaxy with its net angular momentum vector aligned with its short axis would show a “kinematic misalignment” between the projected axes of the rotation and the light, and surveys of elliptical galaxy kinematics have found that such kinematic misalignments are common (Davies & Birkinshaw 1988; Franx, Illingworth, & Heckman 1989; Jedrzejewski & Schechter 1989). However, a kinematic misalignment may also be caused by an *intrinsic* misalignment between the rotational and the short axes because the angular momentum vector of an equilibrium triaxial system can lie anywhere in the plane of the long and short axes (Heiligman & Schwarzschild 1979). Alternatively, the galaxy may not be in equilibrium (due to a recent accretion event or to tidal forces from a satellite galaxy), or it may be a misidentified S0 with a bar (see Merritt 1997a for a review of examples). A statistical analysis of kinematic misalignments in bright ellipticals (Franx, Illingworth, & de Zeeuw 1991) found limits on the mean stellar triaxiality and the mean intrinsic misalignment angle of $\langle T_* \rangle \leq 0.7$ and $\langle \psi_{\text{int}} \rangle \leq 45^\circ$, where the upper bounds for both parameters occurred only for solutions with two widely-separated peaks. Although degeneracies prevented strong constraints on T_* , there were indications for a bimodal population of galaxies, with a large fraction of nearly-oblate, short-axis rotators, and a small fraction of nearly-prolate, long-axis rotators. Tenjes et al. (1993) and Statler (1994a,b, Statler & Fry 1994) have devised methods which invert the projected streamlines of stellar orbits to determine the intrinsic shape of a galaxy, and their initial results also indicate the existence of a bimodal population (Statler, Dutta, & Bak 1997; Bak & Statler 1997).

Theoretical models of halo formation generally produce flattened, prolate-triaxial halos (e.g., Bardeen et al. 1986; Frenk et al. 1988; White & Ostriker 1990; Aguilar & Merritt 1990; Katz 1991; Cannizzo & Hollister 1992; Cole & Lacey 1996). For example, N -body simulations of a small sample of halos by Dubinski (1991, 1992) and Dubinski & Carlberg (1991) found that at 25 kpc they are very flat (mean short axis ratio of $\langle c_d \rangle \simeq 0.42 \pm 0.06$) and nearly-prolate ($\langle T_d \rangle \simeq 0.8 \pm 0.2$). The final halo shapes and angular momenta were very sensitive to the initial cosmological tidal field, and the angular momentum vectors were well-aligned with the short axes, with an average intrinsic misalignment of $\langle \psi_{\text{int}} \rangle \simeq 26^\circ \pm 22^\circ$. Warren et al. (1992) found similar results ($\langle c_d \rangle \simeq 0.62 \pm 0.13$ and $\langle T_d \rangle \simeq 0.68 \pm 0.24$ at 40 kpc), and found that the more massive halos were slightly flatter and more prolate. Again, the angular momentum vector was most commonly aligned with the short axis. We expect dissipative processes to produce baryonic galaxies with shapes that are drastically different from those of their parent halos (e.g., Katz & Gunn 1991; Udry 1993; Navarro & White 1994), but the concomitant effects on the shapes of the halos are unclear. Preliminary simulations suggest that halos become rounder and more oblate through interactions with baryons (Evrard, Summers, & Davis 1994; Dubinski 1994), probably due to the destruction and damping of halo box orbits. Dubinski (1994) found that the flatness and prolateness are reduced relative to a dissipationless model ($c_d \sim 0.6$ versus 0.4, and $T_d \sim 0.4$ -0.5 versus 0.8, at 20 kpc). Late, major mergers of disk galaxies in compact groups may have produced some fraction of the present

population of ellipticals (e.g., Heyl, Hernquist, & Spergel 1994; Weil & Hernquist 1996; Barnes & Hernquist 1996). Although the simulations have not carefully explored the effects of the mergers on the shapes of the dark halos, Weil & Hernquist (1996) suggest that the shapes of remnant halos are rather round and oblate-triaxial, having no correlation with the shapes of the remnant stellar distributions. Current theoretical and observational results thus suggest that the modestly triaxial-oblate luminous parts of elliptical galaxies are embedded in halos which are more prolate, so that there should be a strong gradient with radius in the triaxiality of the mass distribution.

Direct measurements of the shapes of halos are far more difficult than measurements of the shapes of the stellar distributions. Careful examination of the kinematics of polar rings (Arnaboldi et al. 1993), gas disks (Lees 1991; Bertola et al. 1991; Franx, van Gorkom, & de Zeeuw 1994; Plana & Boulesteix 1996; Bureau & Freeman 1997), and planetary nebulae (Hui et al. 1995; Mathieu, Dejonghe, & Hui 1996) have been used to constrain the shapes of both stellar and dark matter potentials. Unfortunately, such tracers are rarely found at large enough galactocentric radii to be helpful for probing the dark matter potential, and it is likely that there are systematic correlations between the shapes of halos and the presence of rings and disks. Gravitational lenses can also be used to directly measure the shapes of mass distributions, and the data appear to require very flat mass distributions. However, the number of lenses is small, and the quantitative effects of external tidal perturbations are not yet understood (King & Browne 1996; Kochanek 1996; Keeton, Kochanek, & Seljak 1997; Witt & Mao 1997). The most promising candidate for directly measuring the intrinsic shapes of nearby halos is high-resolution mapping of the X-ray emission from hot gas in the halo potential. For example, Buote & Canizares (1994, 1996b, 1997; hereafter BC94, BC96b, BC97) examined the radial profiles, position angles, and axis ratios of the X-ray isophotes of the bright, isolated E4 galaxy NGC 720, and found that the shape and the position angle of the potential cannot be produced by the stars. Thus, by using only geometric evidence and the assumption that the gas is in quasi-hydrostatic equilibrium, they showed that the stars must be embedded in a more massive, *flatter*, dark matter halo. For the S0 galaxy NGC 1332, Buote & Canizares (1996a) reached a qualitatively similar conclusion.

X-ray observations can also be used to constrain the triaxialities of halos by searching for X-ray isophote twists. The projection of a triaxial light distribution whose triaxiality varies with radius produces isophotes whose axis orientations vary with radius (see Mihalas & Binney 1981). Isophote twists in the optical surface brightness are common (e.g., Williams & Schwarzschild 1979; Leach 1981), and can be used to constrain the shape of an individual galaxy (Fasano 1995), although care must be taken to rule out intrinsic axis twist caused by other factors (Fasano & Bonoli 1989; Nieto et al. 1992). X-ray emission from a triaxial system can show an analogous isophote twist — as pointed out by Binney (1978) for the case of a galaxy cluster — allowing the triaxiality of an individual galaxy’s potential to be probed. In the simplest case, if a galaxy’s luminous and dark matter distributions are intrinsically aligned and have *constant* but *different* triaxialities, then the projected axes of its X-ray isophotes will twist from small radii, where the potential is dominated by the stellar core, to large radii, where it is dominated by the dark halo. Similarly, as discussed

by BC96b, the radial triaxiality gradients produced in halos by dissipative processes can result in X-ray isophote twists. Here we employ simple models to study the behavior of X-ray twists, and to determine how well they constrain the triaxiality of halos. In §2.1, we use an analytic approximation to find the amplitudes of twists expected for different assumptions about the shapes of galaxies and halos. In §2.2, we numerically calculate and project the X-ray emission for a small sample of models to verify the predictions of the analytic model, and to examine the radial behavior of the twist more closely. In §3, we attempt to model the large twist observed in NGC 720 (BC94, BC96b), and we present our conclusions in §4.

2. CHARACTERISTICS OF X-RAY ISOPHOTE TWISTS

2.1. Analytic Projection of Triaxial Ellipsoids

An ellipsoidal luminosity density $\nu(m^2)$ with constant axis ratios c/a and b/a depends only on the ellipsoidal coordinate $m^2 \equiv X^2/a^2 + Y^2/b^2 + Z^2/c^2$ (hereafter, we will set $a = 1$ for simplicity). When it is projected in the spherical-polar coordinate direction (θ, ϕ) , with the observer's z -axis along the line of sight, its surface brightness can be expressed as a one-dimensional integral of the radial density profile,

$$I(x, y) = \frac{2}{\sqrt{f}} \int_0^\infty \nu(u^2 + m_s^2) du, \quad \text{where}$$

$$f \equiv \sin^2 \theta \left(\cos^2 \phi + \frac{\sin^2 \phi}{b^2} \right) + \frac{\cos^2 \theta}{c^2}, \quad m_s^2 \equiv \frac{1}{f} (Ax^2 + Bxy + Cy^2),$$

$$A \equiv \frac{\cos^2 \theta}{c^2} \left(\sin^2 \phi + \frac{\cos^2 \phi}{b^2} \right) + \frac{\sin^2 \theta}{b^2}, \quad B \equiv \cos \theta \sin 2\phi \left(1 - \frac{1}{b^2} \right) \frac{1}{c^2},$$

$$\text{and } C \equiv \left(\frac{\sin^2 \phi}{b^2} + \cos^2 \phi \right) \frac{1}{c^2}. \quad (1)$$

For $\theta = 0^\circ$, the line of sight is along the short axis; for $\theta = 90^\circ, \phi = 0^\circ$, it is along the long axis; and for $\theta = 90^\circ, \phi = 90^\circ$, it is along the intermediate axis. The surface brightness I is also ellipsoidal, with a constant axis ratio q and a constant minor axis position angle ψ from the projection of the short axis. If the galaxy rotates about its short axis, ψ is equivalent to the kinematic misalignment angle. The axis ratio and the position angle are

$$q^2 = \frac{A + C - \sqrt{B^2 + (A - C)^2}}{A + C + \sqrt{B^2 + (A - C)^2}}, \quad \text{and}$$

$$\tan 2\psi = \frac{B}{A - C} = \frac{T \cos \theta \sin 2\phi}{T(\cos^2 \theta \sin^2 \phi - \cos^2 \phi) + \sin^2 \theta}. \quad (2)$$

Equations 1 and 2 were derived by Binney (1985). The axis ratio $q(b, c, \theta, \phi)$ is a function of the projection angles and both axis ratios of the triaxial ellipsoid, but the position angle $\psi(T, \theta, \phi)$ is a function of only the triaxiality parameter $T \equiv (1 - b^2)/(1 - c^2)$ and the projection angles

(Franx, Illingworth, & de Zeeuw 1991). If we now consider two triaxial distributions whose three-dimensional axes are intrinsically aligned, but which have different triaxialities ($T_1 < T_2$), they are misaligned in projection by the angle $\Delta\psi$, given by

$$\sin 2\Delta\psi = \frac{(T_2 - T_1) \sin^2 \theta \cos \theta \sin 2\phi}{D_2 D_1}, \quad \text{where}$$

$$D_i^2 \equiv T_i^2 \cos^2 \theta \sin^2 2\phi + [T_i(\cos^2 \theta \sin^2 \phi - \cos^2 \phi) + \sin^2 \theta]^2. \quad (3)$$

If the two distributions have the same triaxialities ($T_1 = T_2$), then the misalignment angle is zero ($\Delta\psi = 0$); and if one of the distributions is oblate ($T_1 = 0$), then the misalignment angle is equal to the other distribution's kinematic misalignment angle ($\Delta\psi = \psi_2$).

These expressions for the misalignment angle are applicable to the case of a luminous galaxy embedded in a dark halo, where the two distributions have differing triaxialities, labeled by T_* and T_d . The projected mass will not be aligned with the projected light, an effect which can be important in gravitational lens systems (Keeton, Kochanek, & Seljak 1997). To demonstrate the amplitude of the misalignment for this simple model, Figure 1 shows the misalignment angle as a function of the viewing angles, $\Delta\psi(\theta, \phi)$, for $T_* = 0.25$ and $T_d = 0.75$. Large misalignment angles ($\Delta\psi \gtrsim 45^\circ$) occur when the distribution is viewed near the major axis ($\sin^2 \phi \lesssim 0.05 \cdot \Delta T / T_*$) at intermediate latitudes ($T_* \lesssim \sin^2 \theta \lesssim T_d$).

Figure 2 shows the mean misalignment angle, $\langle \Delta\psi \rangle$, and its dispersion, $\sigma_{\Delta\psi}$, averaged over all viewing angles (θ, ψ), for all possible triaxialities (T_*, T_d). The dispersion $\sigma_{\Delta\psi}$ is comparable to the mean, and $\langle \Delta\psi \rangle$ increases smoothly with ΔT , so that the largest mean misalignments occur when the system consists of a very oblate spheroid and a very prolate spheroid. Figure 2 also illustrates the misalignment angles expected for a naive model of the shapes of galaxies and their halos. If we assume a luminous galaxy with rough shape limits taken from model Ia of Franx, Illingworth, & de Zeeuw (1991), and embed it in a dissipationless dark halo whose shape is taken from the models of Dubinski & Carlberg (1991), we find large typical misalignments, $\langle \Delta\psi \rangle \simeq 18^\circ \pm 20^\circ$. If we use the model for a dissipational halo from Dubinski (1994), the typical misalignment angle drops to $\langle \Delta\psi \rangle \simeq 7^\circ \pm 11^\circ$. In both cases, misalignments much larger and much smaller than the mean are common. Thus, for both galaxy formation models, the projected mass will for some viewing angles show a substantial position angle twist from small radii (where the luminous matter is dominant) to large radii (where the dark matter is dominant). If the X-ray isophotes show the same asymptotic axes as the projected mass, $\langle \Delta\psi \rangle$ will also describe the typical asymptotic X-ray misalignment angles. A full numerical model is required to confirm this assumption and to determine where in radius the isophote twist occurs.

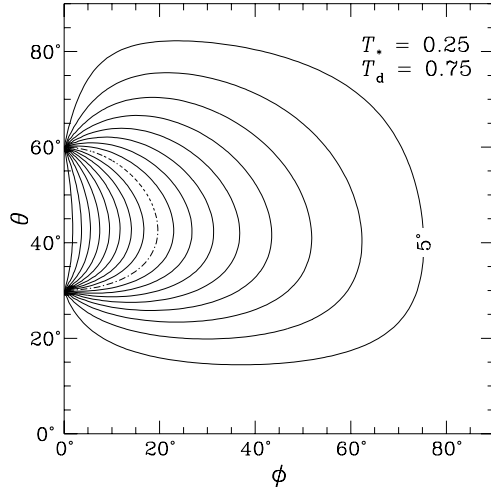


FIG. 1.— The misalignment angle $\Delta\psi$ of two triaxial bodies, for the spherical-polar viewing angles ϕ, θ . The contours are spaced in 5° increments from 5° to 85° , and the solution for $\Delta\psi = 45^\circ$ is highlighted by a dot-dash contour.

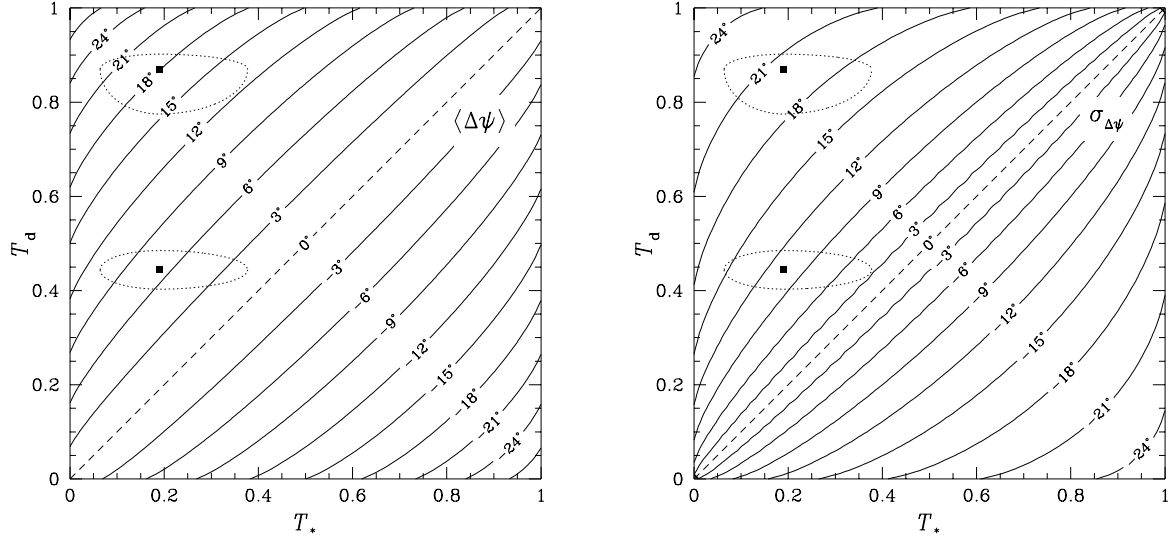


FIG. 2.— Contours of the mean misalignment angle $\langle\Delta\psi\rangle$ (left) and its dispersion $\sigma_{\Delta\psi}$ (right) between two distributions of triaxiality T_* and T_d . As an aid to the eye, rough limits from the literature for stellar and halo triaxialities (T_*, T_d) are shown for a model of galaxy formation which includes dissipation (bottom) and one which does not (top); the squares represent the median values, and the dotted curves show the “one- σ ” limits.

2.2. Numerical Projection of the X-Ray Emission

We model the galaxy as a triaxial “ η -model” distribution of stars (Dehnen 1993; Tremaine et al. 1994) embedded in a triaxial softened isothermal dark matter halo potential, with the axes aligned. The total density, $\rho(\mathbf{r}) = \rho_*(m_*^2) + \rho_d(m_d^2)$, consists of two ellipsoids of the form

$$\rho_d(m_d^2) = \frac{\rho_0}{b_d c_d} \frac{s_d^2}{s_d^2 + m_d^2} \quad \text{and} \quad \rho_*(m_*^2) = \frac{\eta M_*}{4\pi b_* c_*} \frac{s_* m_*^{\eta-3}}{(s_* + m_*)^{\eta+1}}, \quad 0 < \eta \leq 3. \quad (4)$$

An ideal, completely-ionized, single-temperature, non-rotating gas in hydrostatic equilibrium has a density $\rho_g(\mathbf{r}) = \rho_{g0} \exp[-\mu m_p \Phi(\mathbf{r})/k_B T_g]$ and an X-ray emissivity

$$\nu_X(\mathbf{r}) = \alpha(\lambda_X, T_g) \rho_g^2(\mathbf{r}) = \nu_{X0} e^{-2\mu m_p \Phi(\mathbf{r})/k_B T_g} \quad (5)$$

(Cavaliere & Fusco-Femiano 1978), where μm_p is the mean mass per particle, the emissivity constant α (when convolved with the detector’s spectral response) is weakly dependent on the gas temperature T_g , and the potential $\Phi(\mathbf{r})$ is evaluated numerically. The asymptotic profile is $\nu_X(r) \propto r^{-6\beta}$, where $\beta \equiv 4\pi G \rho_0 s_d^2 \mu m_p / 3k_B T_g$. We integrate the X-ray emission along the line of sight to find the surface brightness, $I_X(x, y) = \int_{-\infty}^{\infty} \nu_X(X, Y, Z) dz$, and we find the axis ratios $q(a)$ and the minor axis position angles $\psi(a)$ of the X-ray isophotes by finding the maximum of I_X at each semi-major axis a .

As shown by Buote & Canizares (1994, 1996a), for a gas with any arbitrary temperature profile, the three-dimensional shape of its X-ray emissivity, ν_X , is the same as that of the three-dimensional potential, Φ , in which it lies (i.e., $T_X = T_\Phi$). Although the potential is rounder than the mass, and its axis ratios have a different radial dependence, the projected mass and the projected potential are aligned because they must satisfy the two-dimensional Poisson equation. For an isothermal gas, we find that the X-ray emission ν_X is also roughly aligned with the projected mass ($\sim 1.5^\circ$ typical difference), and thus confirm our assumption that equation 3 and Figure 2 give an accurate asymptotic representation of X-ray isophote twists. Furthermore, by treating the X-ray axis ratios b_X and c_X as those of a perfect triaxial ellipsoid of X-ray emissivity, we can use the analytic expressions (1-2) to find the position angle $\psi_X(a)$ at any radius to an accuracy of $\sim 1^\circ$, and the projected axis ratio $q_X(a)$ to an accuracy of ~ 0.01 .

Figure 3 illustrates in detail the X-ray twists of a realistic galaxy with both stars and a dark halo, for several viewing angles. The stellar component is specified by a Hernquist (1990) model ($\eta = 2$ in equation 4). The relative masses and scale radii of the halo and the stars are set so that the rotation curve along the long axis is flat. The scale radius ratio is $s_*/s_d \simeq 1.8$. The mass ratio of the dark matter and stellar components within the stellar effective radius ($R_{\text{eff}} \simeq 1.8s_*$) is thus ~ 1 , and within $8R_{\text{eff}}$ is ~ 6 . The surface density profiles of galactic X-ray emission can typically be fit by King-type β -models (see Sarazin & Bahcall 1977) with $\beta = 0.4$ - 0.6 (Forman, Jones, & Tucker 1985; Fabbiano 1989), and we set $\beta = 0.4$. The axis ratios of the stellar component are chosen to be $b_* = 0.96$ and $c_* = 0.75$, corresponding to $T_* = 0.18$. The axis ratios of the halo in the dissipationless scenario are $b_d = 0.58$ and $c_d = 0.42$, corresponding to $T_d = 0.81$; and in the dissipational scenario

they are $b_d = 0.85$ and $c_d = 0.62$, corresponding to $T_d = 0.45$. The minor axis position angle of the X-ray isophotes, ψ_X , matches roughly the position angle of the light, ψ_* , at small radii, and that of the halo, ψ_d , at large radii, with a gradual transition at intermediate radii. The radial behavior (e.g., the location and sharpness) of this transition is insensitive to the gas temperature parameter β , and is somewhat sensitive to the viewing angles, the stellar exponent η , the scale radii, and the mass ratio. The half-way point of the twist generally occurs at semi-major axis $a \sim 0.1\text{-}0.4R_{\text{eff}}$ for the dissipationless halo model, and at $\sim 0.4\text{-}0.6R_{\text{eff}}$ for the dissipational halo model. As predicted by the analytic description, there is a large scatter in the twist amplitude, depending on the viewing angles. For the dissipationless halo, the median asymptotic twist is $\Delta\psi_X \sim 15^\circ$, and our small sample shows twists as small as 3° and as large as 45° . For the dissipational halo, the median twist is $\sim 6^\circ$, and twists from 1° to 20° are seen. Note that although the halo begins to dominate the total mass only outside R_{eff} , the X-ray isophote twist can occur much closer to the core. This is because the triaxiality of the X-ray emissivity T_X is not a linear function of the axis ratios (b_X, c_X), and in this case where the stellar potential is nearly oblate, the small amount of additional flattening that is produced by the halo along the intermediate axis is sufficient to alter the triaxiality (and thus the isophote position angle) considerably. With our numerical model, we reappraise the limits from Figure 2 and find that at $3R_{\text{eff}}$, the mean misalignment angle for the dissipationless model is $\langle\Delta\psi_X\rangle \simeq 16^\circ \pm 19^\circ$, and for the dissipational model is $\simeq 5^\circ \pm 8^\circ$.

The axis ratios of the X-ray isophotes are less strongly affected by triaxiality differences and parameter adjustments. For the dissipationless halo, $q_X \sim 0.85\text{-}0.9$ at R_{eff} for most viewing angles, and for the dissipational halo, $q_X \sim 0.9\text{-}0.95$. Figure 4 shows X-ray isophote contours in the central regions of the galaxy for both halo models and some different viewing angles. Note that the larger twists occur for rounder isophotes, whose position angles are more difficult to determine. Although it is not apparent from the figure, the position angle of the X-ray isophotes asymptotically approaches that of the projected halo mass. In many cases we will not be able to resolve the X-ray twist, but we can still recognize its presence and measure its amplitude by observing the misalignment between the stellar and the outer X-ray isophotes.

As a further complication, motivated by observations of the galaxy NGC 720 (BC97), we add a contribution from discrete X-ray sources whose luminosity distribution is directly proportional to the stellar mass distribution ρ_* , and whose total emission is 20% of the gaseous X-ray emission within $5R_{\text{eff}}$. This discrete component significantly modifies the triaxiality of the X-ray emission, and causes the X-ray twist to remain relatively flat to a much larger radius (see Figure 3). The character of the twist also becomes much more sensitive to the galaxy model parameters, including the gas temperature β , once we include a discrete component.

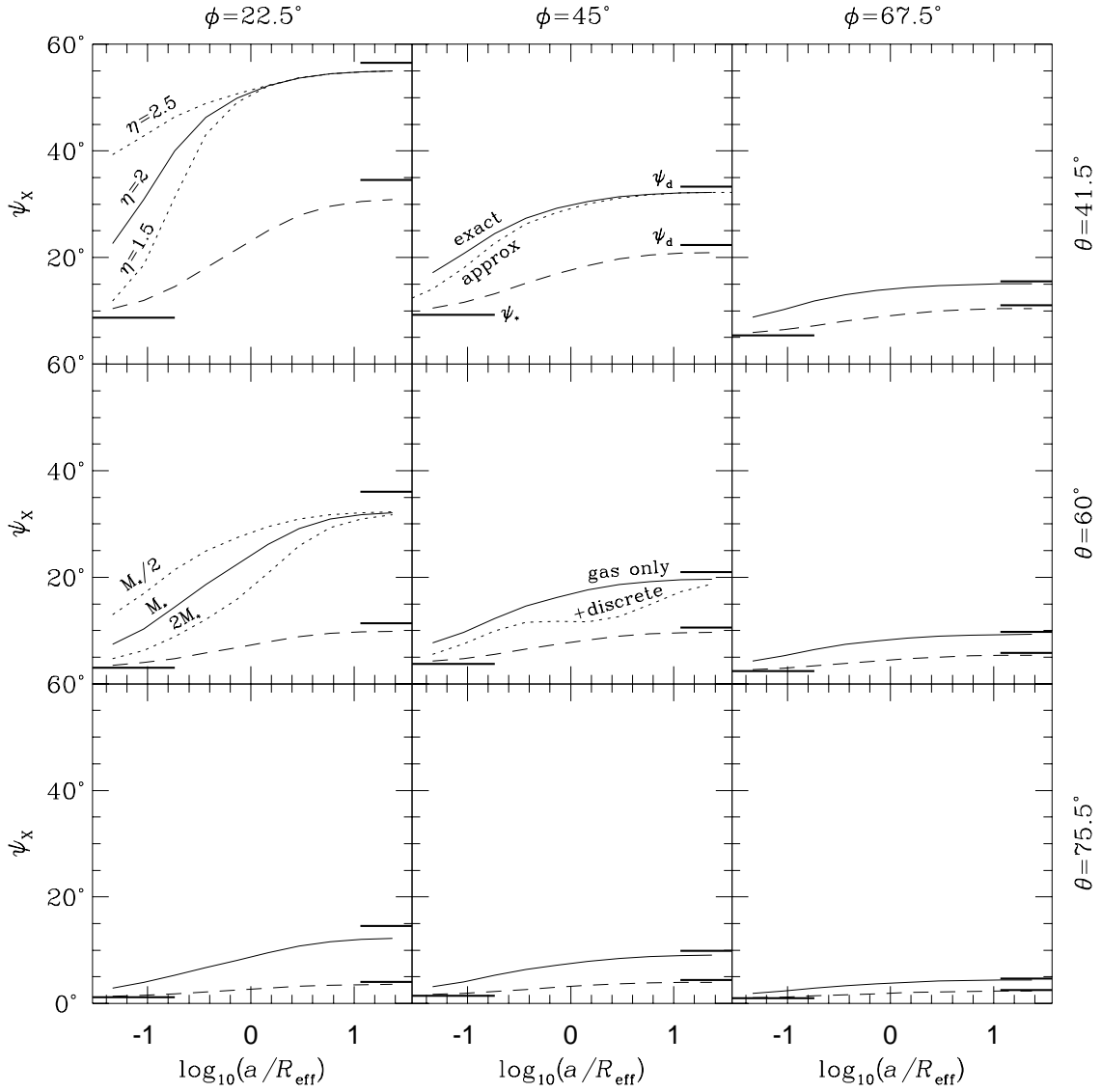


FIG. 3.— The minor-axis position angle of the X-ray isophotes of a model galaxy (measured relative to the projected kinematic axis), as a function of the semi-major axis, for a gridded sample of viewing angles. The solid curves correspond to the dissipationless model, and the dashed curves to the dissipational model. Some special cases are also displayed for the dissipationless model (dotted curves). The center plot shows a case with a discrete source component added. The center left plot shows cases with different stellar component masses, M_* . The top left plot shows cases with different values for the stellar exponent, η . The top center plot shows the analytic approximation for the twist angle. The stellar and halo misalignment angles (ψ_* and ψ_d) are marked (see top center plot for labeling).

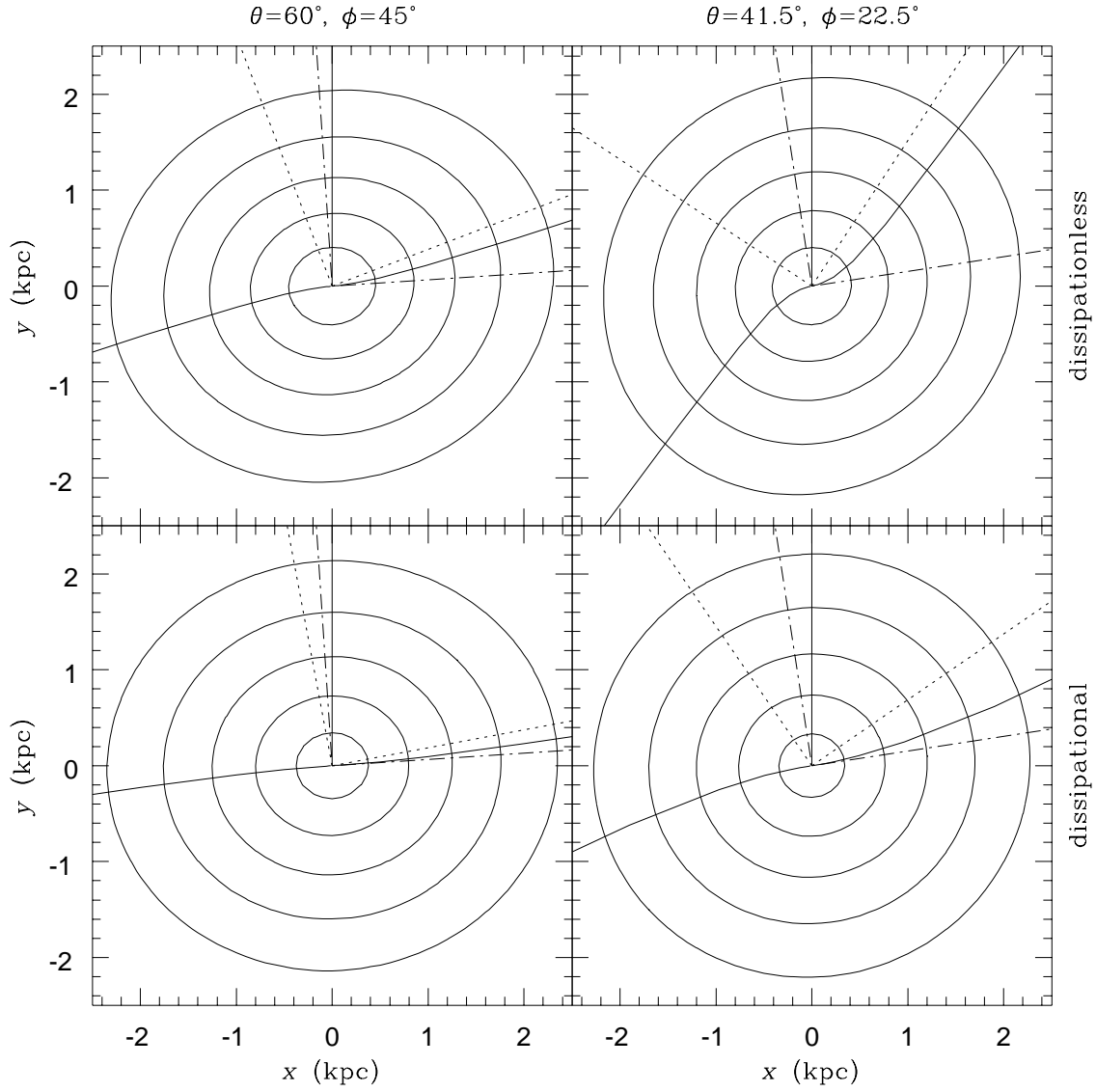


FIG. 4.— X-ray isophotes of two model galaxies, for different viewing angles. The contours are logarithmically spaced, with the central levels omitted for clarity. The major and minor axes of the projected mass are marked for the halo (dotted axes) and for the light (dot-dash axes). The kinematic axis Ψ_k is marked by a vertical solid line. The (twisting) X-ray major axis is shown by a solid line. The top two cases correspond to a model with a halo from the dissipationless scenario, while the bottom cases are from the dissipational scenario. The stellar effective radius is $\simeq 5.4$ kpc.

3. A KNOWN EXAMPLE: NGC 720

Finally, we consider the particular case of NGC 720, an isolated E4 galaxy with bright X-ray emission (Forman, Jones, & Tucker 1985), and no evidence that environmental effects distort its X-ray isophote shapes significantly (BC96b). According to Binney, Davies, & Illingworth (1990), the stellar misalignment angle ψ_* is consistent with zero. Buote & Canizares (BC94, BC96b, BC97) have carefully studied and modeled NGC 720 based on data from *ROSAT*'s PSPC and HRI, and *ASCA*. They found that the X-ray isophotes are significantly elongated ($q_X \sim 0.75$ for $a \simeq 60''$ - $110''$, where $1'' \sim 0.1h_{80}$ kpc), with some indication that the ellipticity decreases at large radii ($q_X \sim 0.8$ - 0.9 for $a \gtrsim 120''$). There is a significant X-ray isophote twist between the the inner and the outer isophotes, where the X-ray major axis position angle Ψ_X is consistent with being aligned with the optical angle Ψ_* at small radii ($\Psi_X \simeq 142^\circ$ for $a \lesssim 60''$), and twists to a different angle at large radii ($\Psi_X \simeq 114^\circ$ for $a \gtrsim 90''$). The emission comes primarily from hot isothermal gas, with a lesser component ($\sim 20\%$) from X-ray binaries (BC97). BC94 demonstrated that the shape alone of the X-ray emission necessitates the presence of an extended dark matter halo, since the potential produced by the stellar distribution is too round to produce the high ellipticity observed for the X-ray emission. BC96b suggested triaxiality of the halo as a possible culprit for the X-ray isophote twist, but they were unable to reproduce the twist using a simple triaxial model in which the intrinsic axis ratios vary with radius according to a power law.

We reinvestigate the hypothesis that triaxiality is responsible for the observed X-ray isophote twist by searching for a reasonable galaxy model whose stellar and halo components produce a radially-varying axis ratio $q_X(a)$ and minor axis position angle $\psi_X(a)$ consistent with those reported for NGC 720. Taking advantage of the fact that we can use the analytic equations (1-2) to find good approximations for q_X and ψ_X , we try to find reasonable values for the parameters $\vec{\xi} = (T_*, c_*, T_d, c_d, \theta, \phi)$ which will give us the observed data $\vec{\delta} = (\psi_*, q_*, \psi_X, q_X)$. We use a Bayesian statistical technique to find the most probable solution, and examine first the case with a dissipationless halo. For our priors, we use Gaussian distributions of the parameters (c_*, c_X, T_*, T_X) , where $\langle c_* \rangle = 0.75 \pm 0.2$, $\langle c_X \rangle = 0.79 \pm 0.08$, $\langle T_* \rangle = 0.2 \pm 0.2$, and $\langle T_X \rangle = 0.7 \pm 0.3$. For the data, we set $\psi_* = 0^\circ \pm 10^\circ$, $q_* = 0.60 \pm 0.05$, $\psi_X = 27^\circ \pm 8^\circ$, and $q_X = 0.75 \pm 0.07$, and we assume that the kinematic axis is intrinsically aligned with the short axis.

Figure 5 illustrates the solutions, showing the total posterior probability of the parameters given the data, $P(\xi_i|\vec{\delta}) = \Sigma_{j \neq i} P(\vec{\xi}|\vec{\delta}) / \Sigma_j P(\vec{\xi}|\vec{\delta})$, where $P(\vec{\xi}|\vec{\delta}) = P(\vec{\xi})P(\vec{\delta}|\vec{\xi})$. The maximum likelihood occurs at $(\theta \simeq 67^\circ, \phi \simeq 42^\circ, c_* \simeq 0.51, c_X \simeq 0.71, T_* \simeq 0.17, T_X \simeq 0.96)$, corresponding to $\psi_* \simeq 2.3^\circ, \psi_X \simeq 21.5^\circ, q_* \simeq 0.62, q_X \simeq 0.81$. This solution is a marginal fit to the data given the errors in the axis ratios and position angles of the X-ray isophotes. The solution for the stellar shape is reasonable — although the optical ellipticity of NGC 720 varies considerably with radius, there is no significant isophote twist (Jedrzejewski, Davies, & Illingworth 1987; Capaccioli, Piotto, & Rampazzo 1988; Peletier et al. 1990; Nieto et al. 1991; Sparks et al. 1991), indicating either that the stellar distribution is very oblate, or that it is triaxial and we are observing it nearly “edge-on”. The X-ray emissivity shape corresponds to a flat, prolate halo with $c_d \simeq 0.34, T_d \simeq 1.0$, which is

consistent with the models of BC94, where $c_d \sim 0.2-0.5$, assuming an edge-on viewing angle and either an oblate or a prolate halo. If we use priors on the halo shape from the dissipational collapse scenario, it is significantly more difficult to fit the data.

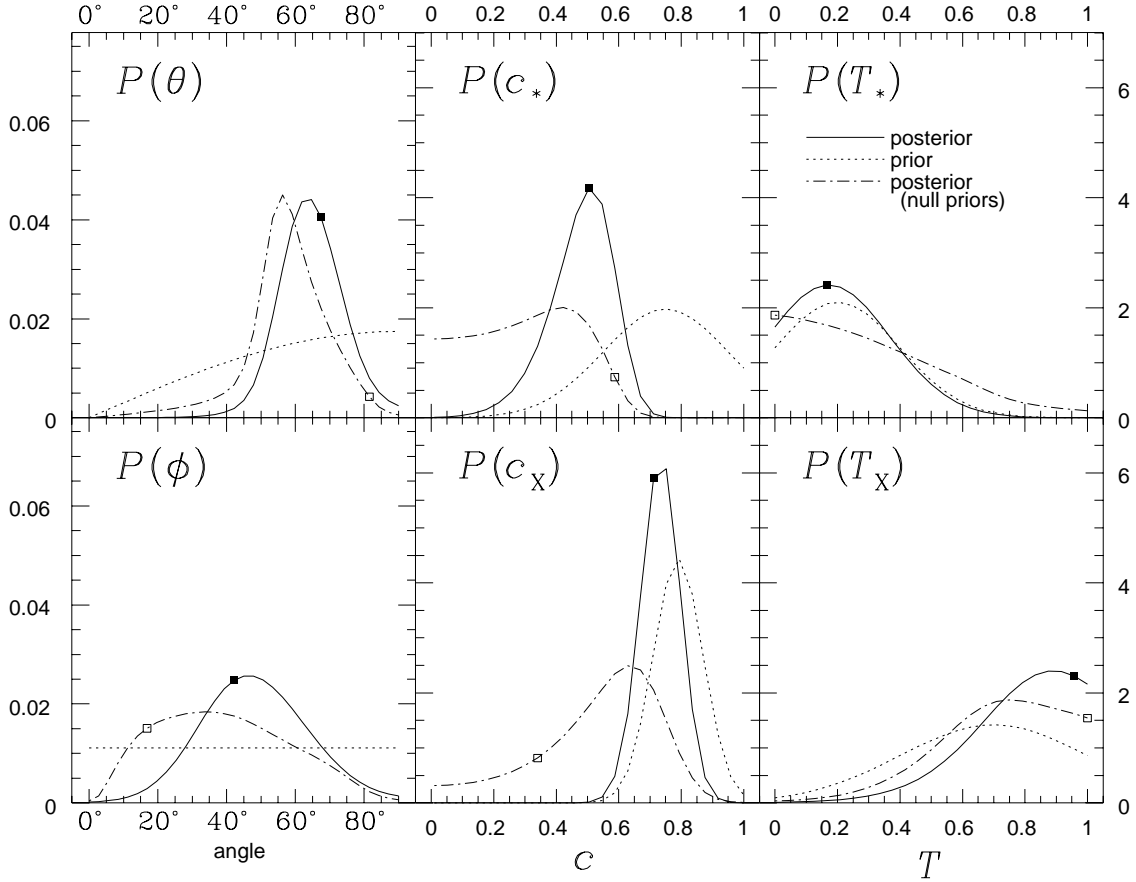


FIG. 5.— The projected likelihood distribution for the model parameters to fit the data for NGC 720. The prior distributions are plotted, as are the posterior distributions which included the priors, and the posterior distributions which did not include the priors (excepting the prior on θ). The squares mark the maximum likelihood solution.

We next use the maximum likelihood model to see if it can reproduce the shapes and orientations of the X-ray isophotes in detail. Since the stellar effective radius is $R_{\text{eff}} \simeq 52''$ (Burstein et al. 1987), we take the scale radius to be $s_* = 28''.6$. After BC94, we set the gas temperature to give a radial profile exponent of $\beta = 0.5$. Since BC94 find that inside $450''$, the ratio of the masses of the halo and the stars $\gtrsim 4$ at 90% confidence, with no upper bound, we use a model with a mass ratio of ~ 0.7 inside R_e and ~ 7 inside $450''$ ($\sim 9R_{\text{eff}}$). From the fits of BC94, we take a typical halo

scale radius to be $s_d = 59''.6$. Figure 6 shows the model X-ray isophotes, and Figure 7 compares the radial variation of the position angle and axis ratio of its projected X-ray emission to the data¹. Although the twist and the ellipticity at large radii are marginally compatible with the data, the twist transition is too gradual and too close to the core. Despite much experimentation with the model parameters, we could not significantly improve our fit to the transition. By adding a discrete source component to the X-ray emission, we can push the transition radius further outward, but it becomes far more difficult to fit the amplitude of the twist. The effects are similar if we compute the twist with the moment method (BC94), or if we allow for substantial rotation of the X-ray emitting gas in the central regions. We thus qualitatively confirm the tentative result of BC96b that it is very difficult for simple models with a radial triaxiality gradient to simultaneously fit both the high ellipticity and the large, abrupt twist of the observed X-ray isophotes.

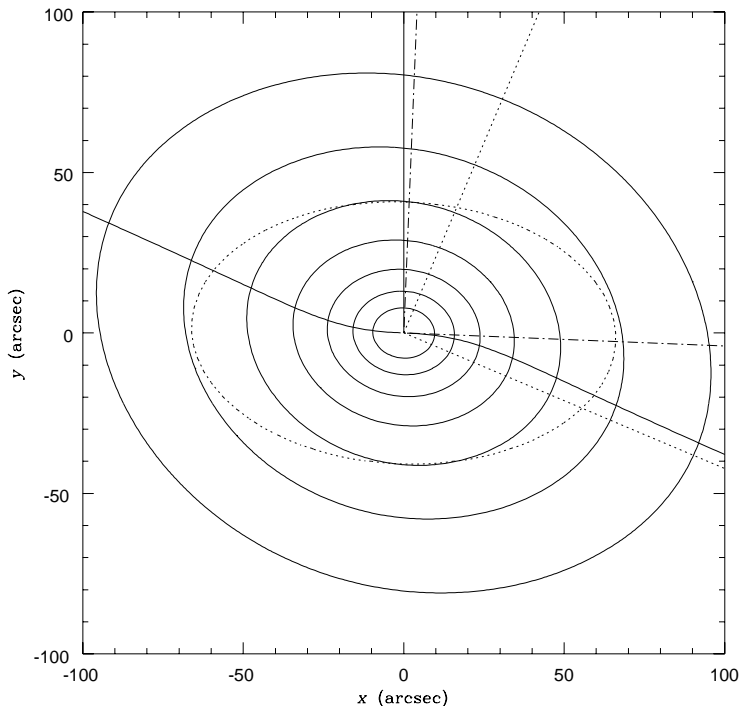


FIG. 6.— X-ray isophotes of our model of NGC 720. (Compare BC94 Fig. 5.) The contours are spaced logarithmically by a factor of two, with the central levels omitted for clarity. The dotted contour shows the stellar surface density isophote at the stellar effective radius. The major and minor axes of the projected mass are marked for the halo (dotted axes) and for the light (dot-dash axes). The kinematic axis Ψ_k is marked by a vertical solid line. The (twisting) X-ray major axis is shown by a solid line.

¹Note that our models measure Ψ_X and q_X along isophotes, while the data measure them using a moment method (compare ϵ_M and ϵ_{iso} from BC94); these do not differ significantly unless there are large radial gradients.

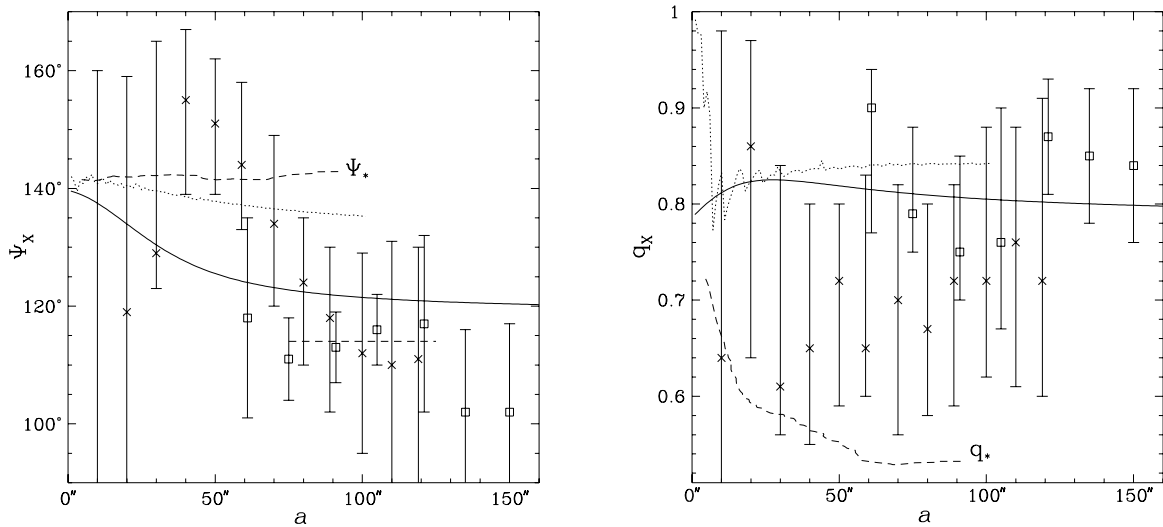


FIG. 7.— The major axis position angle (left) and the axis ratio (right) of the X-ray isophotes as a function of the semi-major axis. Our best-fit model is shown, where the parameters are calculated on isophotes (solid curves) and using a moment method (dotted curves), and the data are shown with their 90% confidence limits (for clarity, data points at the same radius are offset slightly in radius). The *PSPC* data are indicated by squares, and the *HRI* data by crosses. The position angle (Ψ_*) and the axis ratio (q_*) of the stellar isophotes are marked by dashed lines (taken from Jedrzejewski, Davies & Illingworth 1987; Capaccioli, Piotto, & Rampazzo 1988; Peletier et al. 1990; Sparks et al. 1991), as is the approximate position angle of the outer X-ray isophotes.

4. CONCLUSIONS

Current observational evidence indicates that the stellar parts of elliptical galaxies are modestly flattened and close to oblate, while current theories for the formation of galaxies suggest that the halos are more flattened and more prolate. The extent of this shape difference depends on the interactions between baryons and dissipationless dark matter during galaxy formation, but all current models imply that the mass distribution of an early type galaxy increases in flatness and prolateness with radius. There is already some evidence from the flatness of X-ray isophotes (Buote & Canizares 1994, 1996a) and from gravitational lens models (King & Browne 1996; Kochanek 1996) that the typical mass distribution may be flatter than the luminosity distribution. A difference in triaxiality between luminous galaxies and their dark halos is detectable through misalignments of gravitational lenses with their stellar distributions, and is a natural explanation for the second shear axis that is necessary to fit lensing models, although intrinsic misalignments and external tidal shear sources are also viable explanations (Keeton, Kochanek, & Seljak 1997). Such a triaxiality difference also produces X-ray isophote twists (Binney 1978; Buote & Canizares 1996b).

We examined the behavior of X-ray isophote twists using several simple models of a luminous galaxy of constant triaxiality embedded in an intrinsically-aligned dark halo of a different triaxiality. A simple analytic approximation gives accurate estimates of the asymptotic position angles of the X-ray isophotes, but predicting the detailed radial behavior of the twist requires numerical simulations. For a reasonable model of a galaxy and halo, we find that the X-ray isophote position angle makes a gradual transition from the center of the galaxy, where it is aligned with the position angle of the optical isophotes, to the periphery, where it is aligned with the position angle of the projected halo mass. The “half-way” point of the twist occurs well inside the stellar effective radius ($\sim 0.1-0.6 R_{\text{eff}}$), and is not detectable given present X-ray resolution limits, but the misalignment of the X-ray isophotes at large radii with the stellar isophotes is more easily observable. By examining the amplitude of the misalignment for a large population of galaxies, we can in principle distinguish between alternative models for the halo shapes. The very prolate halos predicted by dissipationless collapse simulations should produce mean misalignments of $\langle \Delta\psi_X \rangle \simeq 16^\circ \pm 19^\circ$ at $\sim 3R_{\text{eff}}$, while the more oblate halos predicted by simulations which include baryonic dissipation should produce smaller misalignments ($\simeq 5^\circ \pm 8^\circ$). In practice, measurements of these twists will be difficult because the twist angles are small, the X-ray isophotes are fairly round ($\langle q_X \rangle \sim 0.9$), and the number of isolated, nearby X-ray galaxies is limited. Our results are not very sensitive to the parameters of the model, but the presence of a discrete source component can modify the detailed properties of the twist and should be included in any statistical test. Note that while we scaled our models to match the halo shapes predicted by simulations, *any* mass distribution with a strong radial triaxiality gradient will produce an X-ray isophote twist when observed from the proper angles. For example, the disruption of box orbits by a central stellar cusp can cause the central parts of an elliptical galaxy to become more oblate than the outer parts due to the longer time scales for scattering and phase mixing of the outer orbits (e.g. Merritt 1997b), leaving a twisting signature in the X-ray isophote position angles.

We attempted to model the observed X-ray twist of the bright, isolated E4 galaxy NGC 720 (BC94, BC96b), whose X-ray isophotes are strongly flattened, and show a large, abrupt position angle twist of $\sim 30^\circ$ at $\sim 1-2 R_{\text{eff}}$. While a model halo from the dissipationless scenario fits the data better than does a halo from the dissipational scenario, it is in both scenarios difficult to reproduce both the twist behavior and the isophote flatness using reasonable parameters for the galaxy and halo. The simplest explanation for NGC 720 is that the halo and the stars are intrinsically misaligned. Such an intrinsic misalignment may arise naturally for a halo which forms by dissipationless collapse, or it may be caused by late-history major mergers. Whether caused by triaxiality or by intrinsic misalignment, the shapes and orientations of stellar and X-ray isophotes are important fossil clues to the formation history of galaxies.

We thank David Buote and Christine Jones for their helpful comments. CSK is supported by NSF grant AST-9401722 and NASA ATP grant NAG5-4062.

REFERENCES

- Aguilar, L. A., & Merritt, D. 1990, *ApJ*, 354, 33
- Arnaboldi, M., Capaccioli, M., Cappellaro, E., Held, E. V., & Sparke, L. S. 1993, *A&A*, 267, 21
- Bak, J., & Statler, T. S. 1997, in *Proceedings of the Second Stromlo Symposium, The Nature of Elliptical Galaxies*, ed. M. Arnaboldi, G. S. Da Costa, & P. Saha (San Francisco: ASP), 86
- Bardeen, J. M., Bond, J. R., Kaiser, N., & Szalay, A. S. 1986, *ApJ*, 304, 15
- Barnes, J. E., & Hernquist, L. 1996, *ApJ*, 471, 115
- Bertola, F., Bettoni, D., Danziger, J., Sadler, E., Sparke, L., & de Zeeuw, T. 1991, *ApJ*, 373, 369
- Binney, J. 1978, *Comments on Astrophysics*, 8, 27
- Binney, J. 1985, *MNRAS*, 212, 767
- Binney, J., Davies, R. L., & Illingworth, G. D. 1990, *ApJ*, 361, 78
- Binney, J., & Tremaine, S. 1987, *Galactic Dynamics* (Princeton: Princeton Univ. Press)
- Buote, D. A. & Canizares, C. R. 1994, *ApJ*, 427, 86 (BC94)
- Buote, D. A. & Canizares, C. R. 1996a, *ApJ*, 457, 177
- Buote, D. A. & Canizares, C. R. 1996b, *ApJ*, 468, 184 (BC96b)
- Buote, D. A. & Canizares, C. R. 1997, *ApJ*, 474, 650 (BC97)
- Bureau, M., & Freeman, K. 1997, in *Proceedings of the Second Stromlo Symposium, The Nature of Elliptical Galaxies*, ed. M. Arnaboldi, G. S. Da Costa, & P. Saha (San Francisco: ASP), 93
- Burstein, D., Davies, R. L., Dressler, A., Faber, S. M., Stone, R. P. S., Lynden-Bell, D., Terlevich, R. J., & Wegner, G. 1987, *ApJS*, 64, 601
- Busarello, G., Longo, G., & Feoli, A. 1992, *A&A*, 262, 52
- Cannizzo, J. K., & Hollister, T. C. 1992, *ApJ*, 400, 58
- Capaccioli, M., Caon, N., & D’Onofrio, M. 1992, *MNRAS*, 259, 323
- Capaccioli, M., Piotto, G., & Rampazzo, R. 1988, *AJ*, 96, 487
- Cavaliere, A., & Fusco-Femiano, R. 1978, *A&A*, 70, 677
- Cole, S., & Lacey, C. 1996, *MNRAS*, 281, 716
- Contopoulos, G. 1956, *Zs. Ap.*, 39, 126
- Davies, R. L., & Birkinshaw, M. 1988, *ApJS*, 68, 409
- Dehnen, W. 1993, *MNRAS*, 265, 250
- Dubinski, J. 1991, Ph.D. thesis, Univ. of Toronto
- Dubinski, J. 1992, *ApJ*, 401, 441

- Dubinski, J. 1994, *ApJ*, 431, 617
- Dubinski, J., & Carlberg, R. G. 1991, *ApJ*, 378, 496
- Evrard, A. E., Summers, F. J., & Davis, M. 1994, *ApJ*, 422, 11
- Fabbiano, G. 1989, *ARA&A*, 27, 87
- Fasano, G. 1995, in *ASP Conf. Ser.* 86, *Fresh Views of Elliptical Galaxies*, ed. A. Buzzoni, A. Renzini, & A. Serrano (Provo: ASP), 37
- Fasano, G., & Bonoli, C. 1989, *A&AS*, 79, 291
- Fasano, G., & Vio, R. 1991, *MNRAS*, 249, 629
- Forman, W., Jones, C., & Tucker, W. 1985, *ApJ*, 293, 102
- Franx, M., Illingworth, G., & de Zeeuw, T. 1991, *ApJ*, 383, 112
- Franx, M., Illingworth, G., & Heckman, T. 1989, *ApJ*, 344, 613
- Franx, M., van Gorkom, J. H., & de Zeeuw, T. 1994, *ApJ*, 436, 642
- Frenk, C. S., White, S. D. M., Davis, M., & Efstathiou, G. 1988, *ApJ*, 327, 507
- Heiligman, G., & Schwarzschild, M. 1989, *ApJ*, 233, 872
- Hernquist, L. 1990, *ApJ*, 356, 359
- Heyl, J. S., Hernquist, L., & Spergel, D. N. 1994, *ApJ*, 427, 165
- Hui, X., Ford, H. C., Freeman, K. C., & Dopita, M. A. 1995, *ApJ*, 449, 592
- Jedrzejewski, R. I., Davies, R. L., & Illingworth, G. D. 1987, *AJ*, 94, 1508
- Jedrzejewski, R., & Schechter, P. L. 1989, *AJ*, 98, 147
- Jørgensen, I., & Franx, M. 1994, *ApJ*, 433, 553
- Katz, N. 1991, *ApJ*, 368, 325
- Katz, N., & Gunn, J. E. 1991, *ApJ*, 377, 365
- King, L. J., & Browne, I. W. A. 1996, *MNRAS*, 282, 67
- Keeton, C. R., Kochanek, C. S., & Seljak, U. 1997, *ApJ*, 482, 604
- Kochanek, C. S. 1996, *ApJ*, 473, 595
- Kormendy, J., & Bender, R. 1996, *ApJ*, 464, L119
- Lambas, D. G., Maddox, S. J., & Loveday, J. 1992, *MNRAS*, 258, 404
- Leach, R. 1981, *ApJ*, 248, 485
- Lees, J. F. 1991, in *Warped Disks and Inclined Rings around Galaxies*, ed. S. Casertano, P. D. Sackett, & F. H. Briggs, (Cambridge: Cambridge Univ. Press), 50
- Mathieu, A., Dejonghe, H., & Hui, X. 1996, *A&A*, 309, 30

- Merritt, D. 1997a, in Proceedings of the Second Stromlo Symposium, The Nature of Elliptical Galaxies, ed. M. Arnaboldi, G. S. Da Costa, & P. Saha (San Francisco: ASP), 32
- Merritt, D. 1997b, *ApJ*, [astro-ph/9701154](#)
- Mihalas, D., & Binney, J. 1981, *Galactic Astronomy* (New York: Freeman)
- Navarro, J. F., & White, S. D. M. 1994, *MNRAS*, 267, 401
- Nieto, J.-L., Bender, R., Poulain, P., & Surma, P. 1992, *A&A*, 257, 97
- Nieto, J.-L., Poulain, P., & Davoust, E. 1994, *A&A*, 283, 1
- Nieto, J.-L., Poulain, P., Davoust, E., & Rosenblatt, P. 1991, *A&AS*, 88, 559
- Peletier, R. F., Davies, R. L., Illingworth, G. D., Davis, L. E., & Cawson, M. 1990, *AJ*, 100, 1091
- Plana, H., & Boulesteix, J. 1996, *A&A*, 307, 391
- Ryden, B. S. 1992, *ApJ*, 396, 445
- Ryden, B. S. 1996, *ApJ*, 461, 146
- Sarazin, C. L., & Bahcall, J. N. 1977, *ApJS*, 34, 451
- Sparks, W. B., Wall, J. V., Jordan, P. R., Thorne, D. J., & van Breda, I. 1991, *ApJS*, 76, 471
- Statler, T. S. 1994a, *ApJ*, 425, 458
- Statler, T. S. 1994b, *ApJ*, 425, 500
- Statler, T. S., Dutta, S. N., & Bak, J. 1997, in Proceedings of the Second Stromlo Symposium, The Nature of Elliptical Galaxies, ed. M. Arnaboldi, G. S. Da Costa, & P. Saha (San Francisco: ASP), 75
- Statler, T. S., & Fry, A. M. 1994, *ApJ*, 425, 481
- Tenjes, P., Busarello, G., Longo, G., & Zaggia, S. 1993, *A&A*, 275, 61
- Tremaine, S., Richstone, D. O., Byun, Y.-I., Dressler, A., Faber, S. M., Grillmair, C., Kormendy, J., & Lauer, T. R. 1994, *AJ*, 107, 634
- Tremblay, B., & Merritt, D. 1995, *AJ*, 110, 1039
- Tremblay, B., & Merritt, D. 1996, *AJ*, 111, 2243
- Udry, S. 1993, *A&A*, 268, 35
- Warren, M. S., Quinn, P. J., Salmon, J. K., & Zurek, W. H. 1992, *ApJ*, 399, 405
- Weil, M. L., & Hernquist, L. 1996, *ApJ*, 460, 101
- White, S. D., & Ostriker, J. P. 1990, *ApJ*, 349, 22
- Williams, T. B., & Schwarzschild, M. 1979, *ApJ*, 227, 56
- Witt, H. J., & Mao, S. 1997, *MNRAS*, [astro-ph/9702021](#)